A Two-Year Cloud Climatology for the Southern Great Plains Site

R. T. Marchand, T. P. Ackerman, and E. E. Clothiaux
Pennsylvania State University
University Park, Pennsylvania

Introduction

The addition of the millimeter cloud radar to the suite of instruments at the Southern Great Plains (SGP) site has provided the necessary observations to produce a cloud climatology. Using algorithms developed by our research group, data from the radar are combined with data from the Belfort ceilometer and micropulse lidar to determine cloud occurrence and location. This time series can be analyzed to get monthly and seasonal values of cloud occurrence, cloud fraction, and many other statistics. In this paper, we present a short synopsis of results for 25 months of data.

Basic Statistics

Perhaps the most basic statistic we can generate is the relative frequency of occurrence of clouds. That is, for a given period of time (one month in this figure) how often is a cloud observed above the radar or lidar relative to the length of time data was acquired. Figure 1 shows that if one was looking up in 1997 one was more likely to see a cloud directly over head than in 1998, especially during the summer period. One can further categorize the clouds as Low clouds (i.e., any detection between 0 km and 3 km), Mid-Level clouds (3 km to 7 km), and High clouds (>7 km). (For example, a cloud that fills the entire atmospheric column is considered to have low, mid, and high clouds present.) Figure 1 shows that much of the reduction in cloudiness between summer 1997 and summer 1998 was due to a reduction in high cirrus clouds.

Taking advantage of the full radar vertical resolution and the ability of the radar to penetrate clouds, Figure 2(a) shows the relative frequency of occurrence of clouds versus and Figure 2(b) shows the distribution of cloud thickness on a seasonal scale. The thickness distribution uses bins which are 500 meters wide. (Lidar data is used in estimating the lowest cloud boundary, and clouds that were only detected by the lidar are considered to have a thickness of less than 250 meters.) As in Figure 1, Figure 2(a) shows a reduction in all clouds in summer 1998 relative to summer 1997 but especially in high clouds. Other interesting features include a seasonal shift in the height of the high cloud peak and the very strong increase in low clouds in the winter of 1997-1998 over the winter of 1996-1997 (the later is likely related to the strong El Nino at that time). Figure 2(b) shows that most clouds tend to be between 250 meters and 750 meters thick. The only season that departed from this trend was summer 1997. A detailed examination of summer 1997 revealed that a large number of small broken cirrus elements are responsible for this reduction.

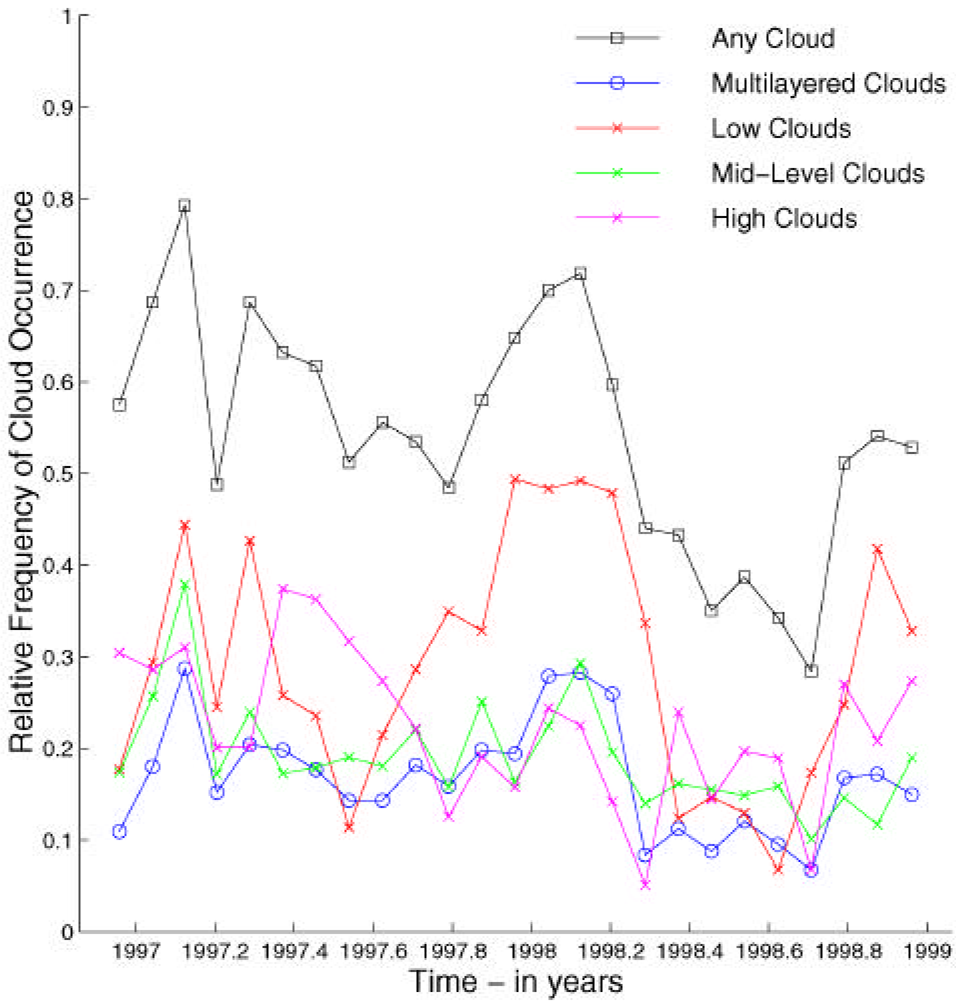

Figure 1.

Each of the 25 months of data that have been examined thus far show some unique characteristics. Figure 3 is the same as Figure 2 only restricted to the months of December 1996, December 1997, and December 1998. Each December is characteristically different. 1997 shows almost no high clouds and large numbers of low clouds. 1996 and 1998 show similar amounts of high clouds (although 1996 had somewhat higher and more broken clouds), but 1998 shows more and thicker low clouds. (As a side note, the radar operational modes were changed after December 1996 to improve their ability to detect low clouds. Hence, Figure 4(a) may not have captured all of the low cloud structure. However, the lidar data from this period also show fewer clouds in this region.)

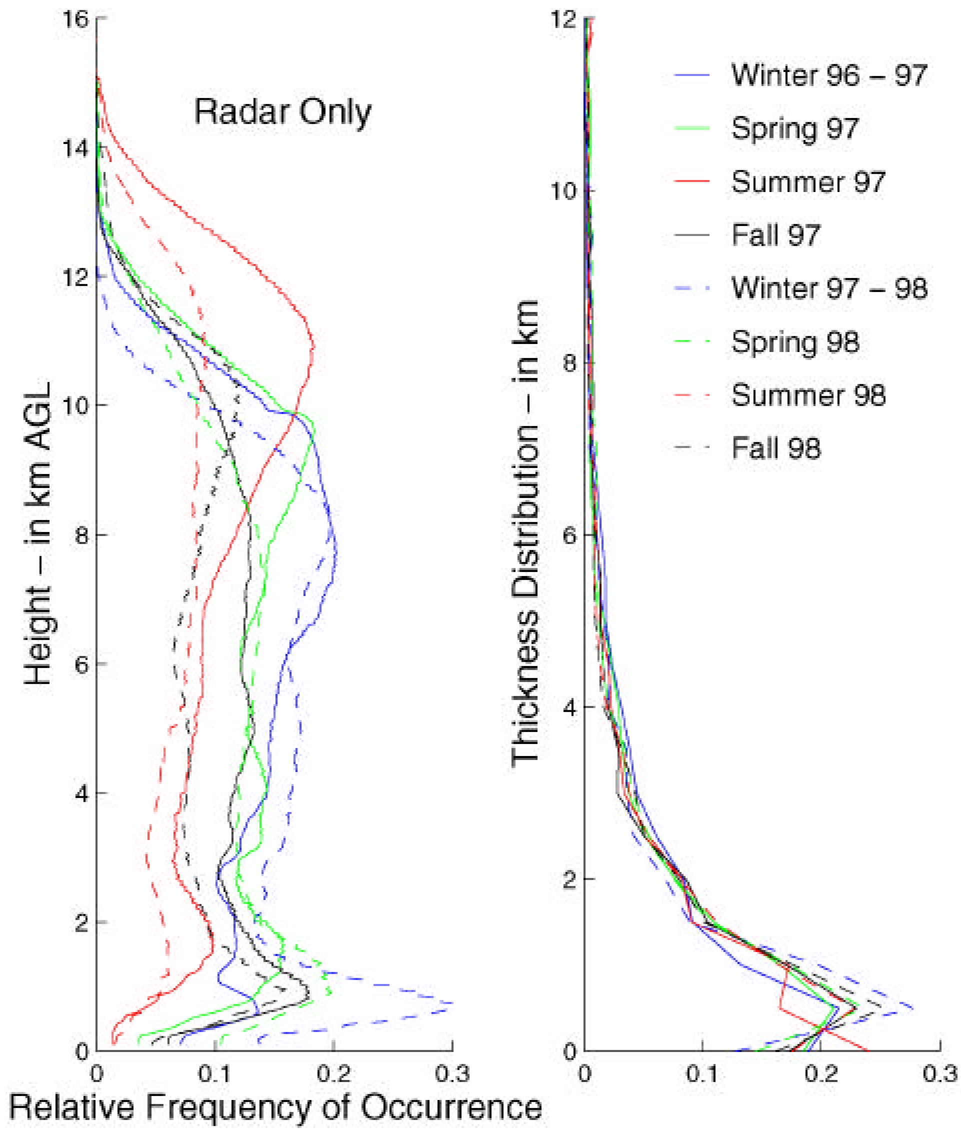

Radar Only
Height – in km AGL
Relative Frequency of Occurrence
Thickness Distribution – in km
Winter 96 – 97
Spring 97
Summer 97
Fall 97
Winter 97 – 98
Spring 98
Summer 98
Fall 98
0
2
4
6
8
10
12
14
16
0.1
0.2
0.3

Figure 2.

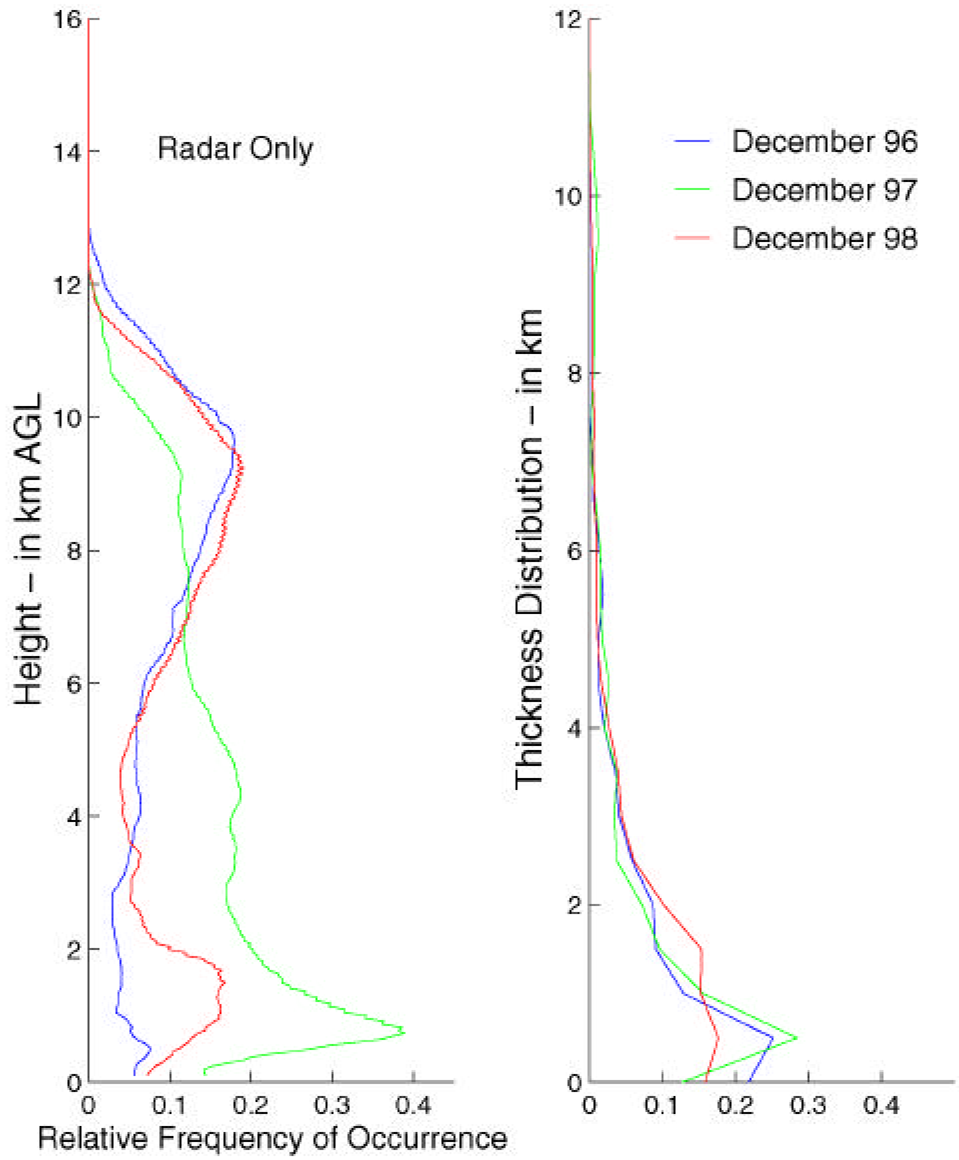
Radar Only
Height – in km AGL
Relative Frequency of Occurrence
Thickness Distribution – in km
December 96
December 97
December 98
0
2
4
6
8
10
12
14
16
0.1
0.2
0.3
0.4

Figure 3.

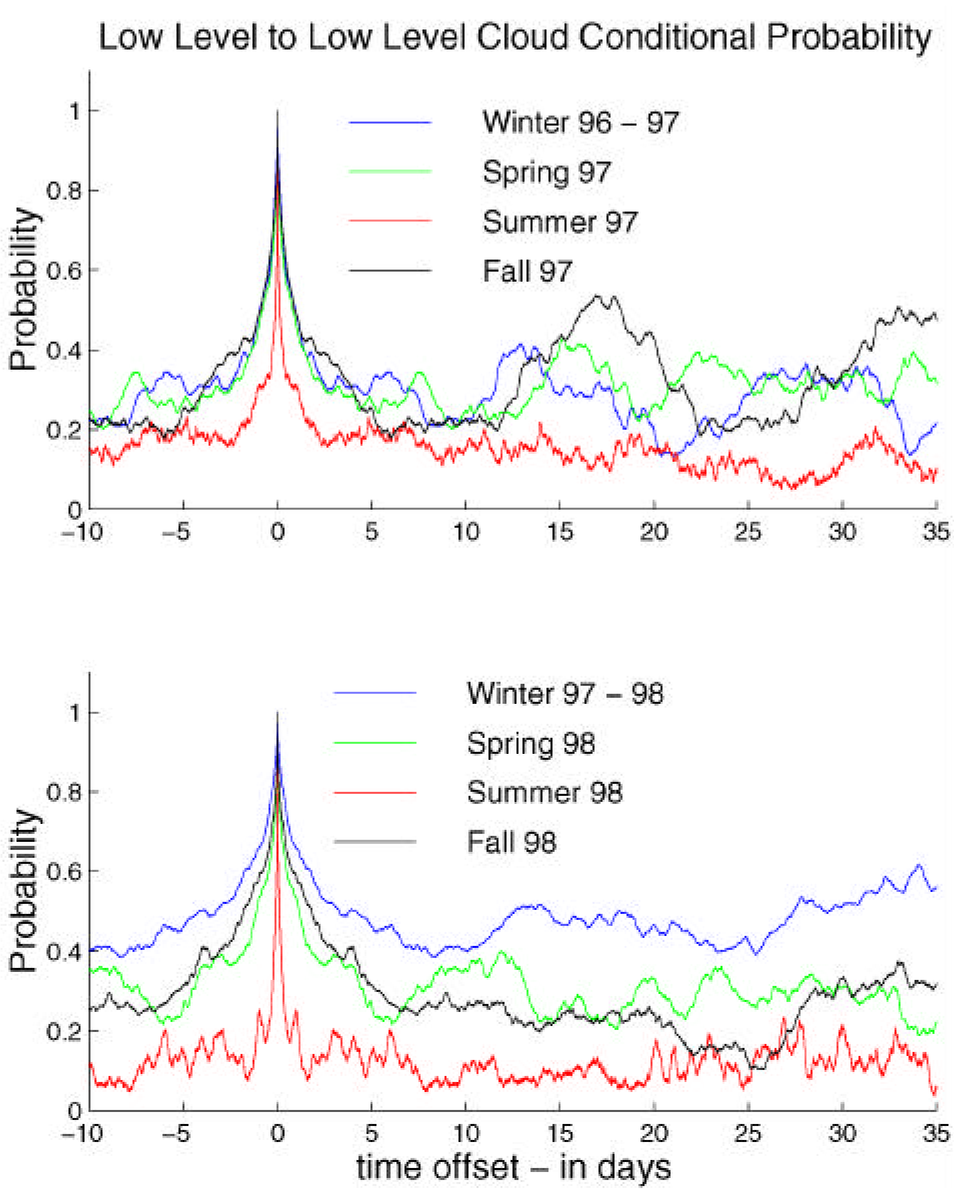

Figure 4.

Conditional Probability

The statistics described in the previous section are single-point statistics. That is, they do not address the persistence associated with cloud and other hydrometeors. For example, given there is a cloud at some time t=0, what is the probability that there will be a cloud at some later time? Figure 1 plots an estimate of this conditional probability for low clouds. That is, when a radar detection between 0 km and 3 km occurs (at or above the lidar cloud base), how often is there also a detection half a day, or a day, or five days later?

At t=0, this conditional probability (which is equivalent to the autocorrelation or self-structure function) must be 1 and the width of the peak around t=0 is an indication of the duration of low cloud events. Variations in the conditional probability at time offsets greater than a few days are indicative of the regularity of synoptic scale weather systems. Fall 1997 (solid black line), for example, shows a strong 16-day periodicity whereas neither summer season shows any significant structure.

The conditional probability estimate for low clouds (0 km to 3 km) with high clouds (>7 km) is show in Figure 5. The most notable features observed in these plots is the asymmetry around t=0 and the position and strength of the peak. That is, this figure shows that one is more likely to observe high clouds before low cloud will be observed.

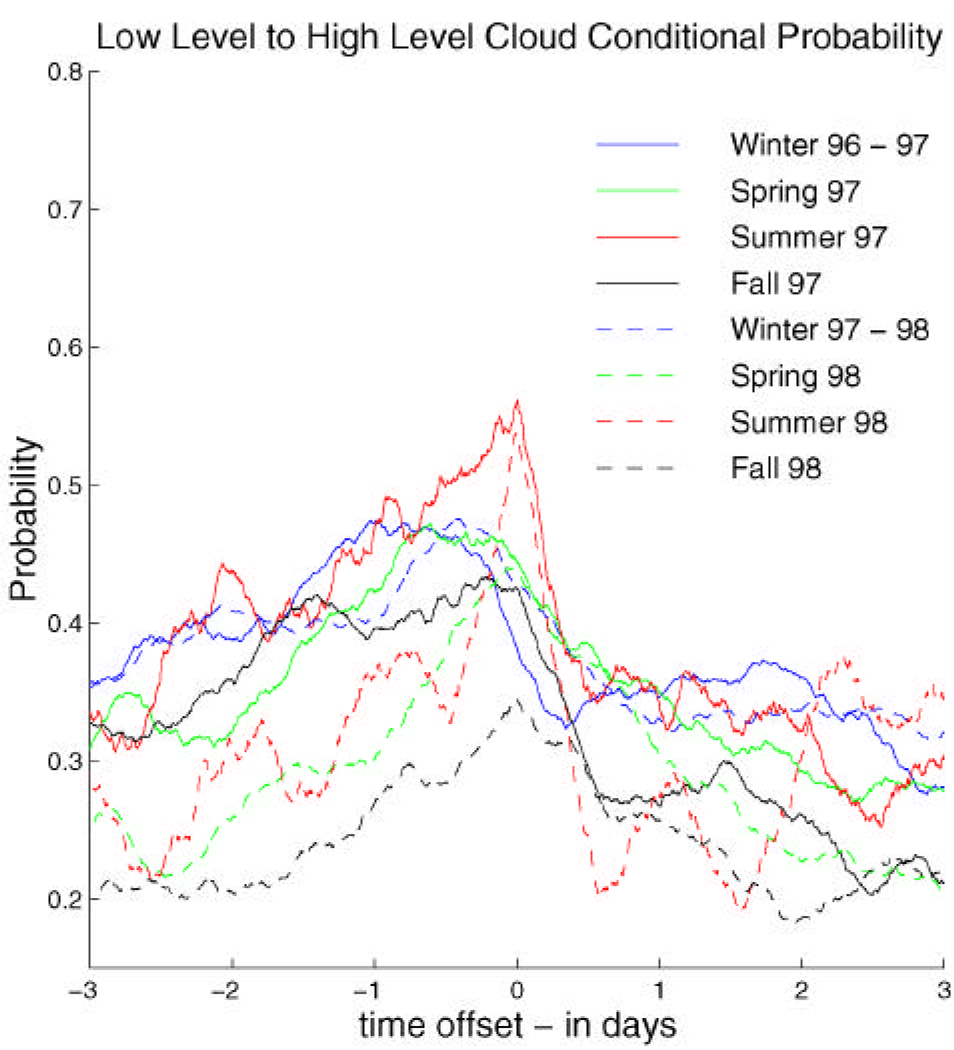

Figure 5.

Application in Analysis of Satellite Data

One of the purposes for creating this cloud database is to use it in evaluating satellite retrievals. Figure 6 shows images of two experimental POLDER (POLarization and Directionality of the Earth's Reflectances) retrievals we are currently studying in cooperation with Jerome Riedi at the Laboratoire d'Optique Atmosphérique Université de Lille. POLDER was an instrument on board the ADEOS satellite, and there are currently plans for a second instrument to fly onboard ADEOS II in a few years. The POLDER instrument collected image data at nine wavelengths between 443 nm and 910 nm. At three wavelengths (443 nm, 670 nm, and 865 nm), a complete set of polarized measurements were made.

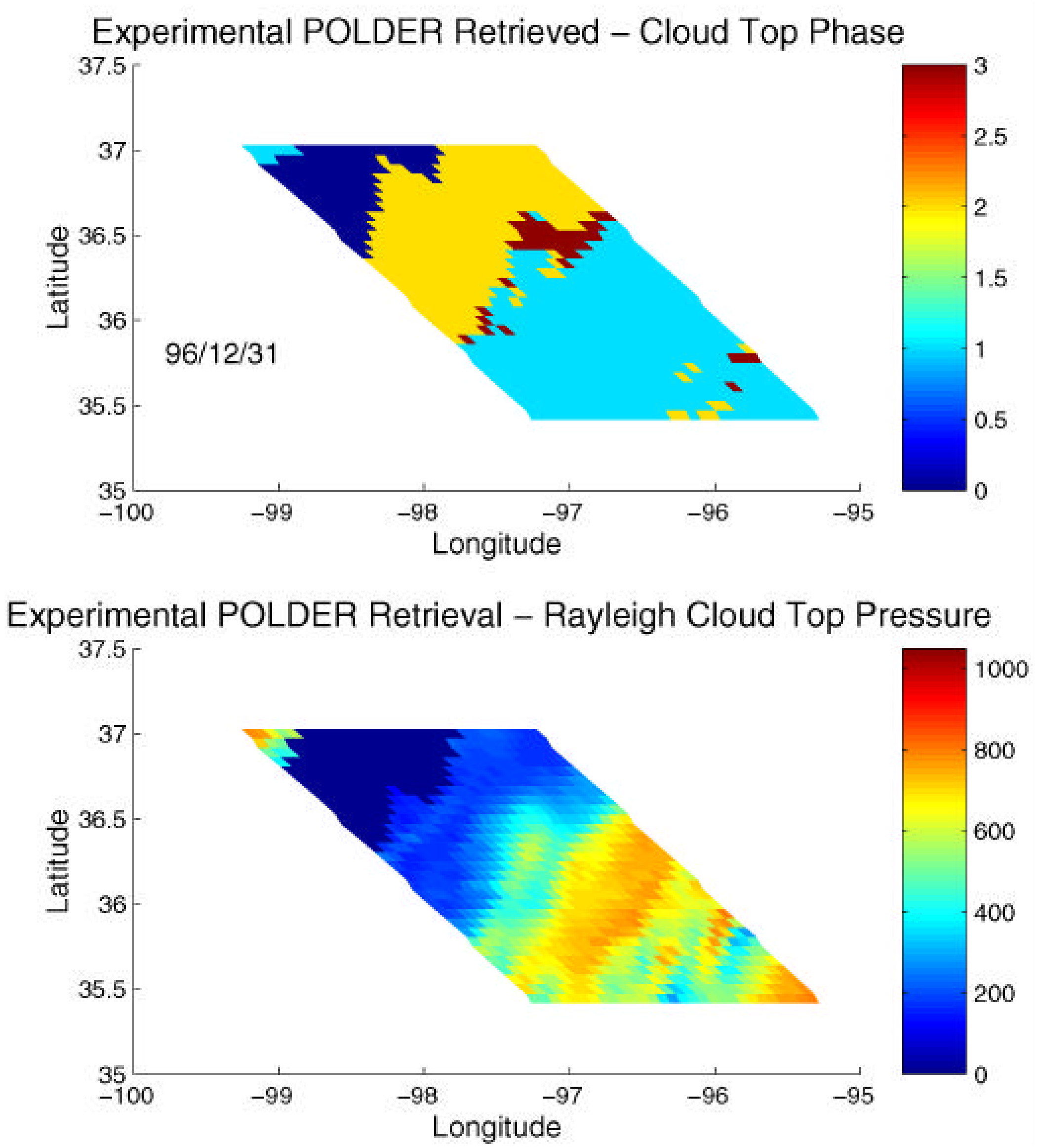

Figure 6.

In Figure 6, the top panel shows an example of the cloud top phase and the bottom panel shows cloud top pressure. In both figures, the displayed region is 30 pixels x 30 pixels centered on the Atmospheric Radiation Measurement (ARM) SGP Cloud and Radiation Testbed (CART) site with a pixel resolution of approximately 6 km. These particular retrievals are computed from the polarization ratios at 443 nm and 865 nm. Figure 7 compares radar-estimated and POLDER-estimated cloud fraction (top panel) and cloud top pressure (bottom panel) for the month of December 1996. The bottom panel indicates the radar-derived cloud top pressures are greater than the corresponding POLDER estimates for low clouds but is less than POLDER estimates for high clouds. I should stress that this is just our first look at this data, and we expect to learn a great deal in the coming months.

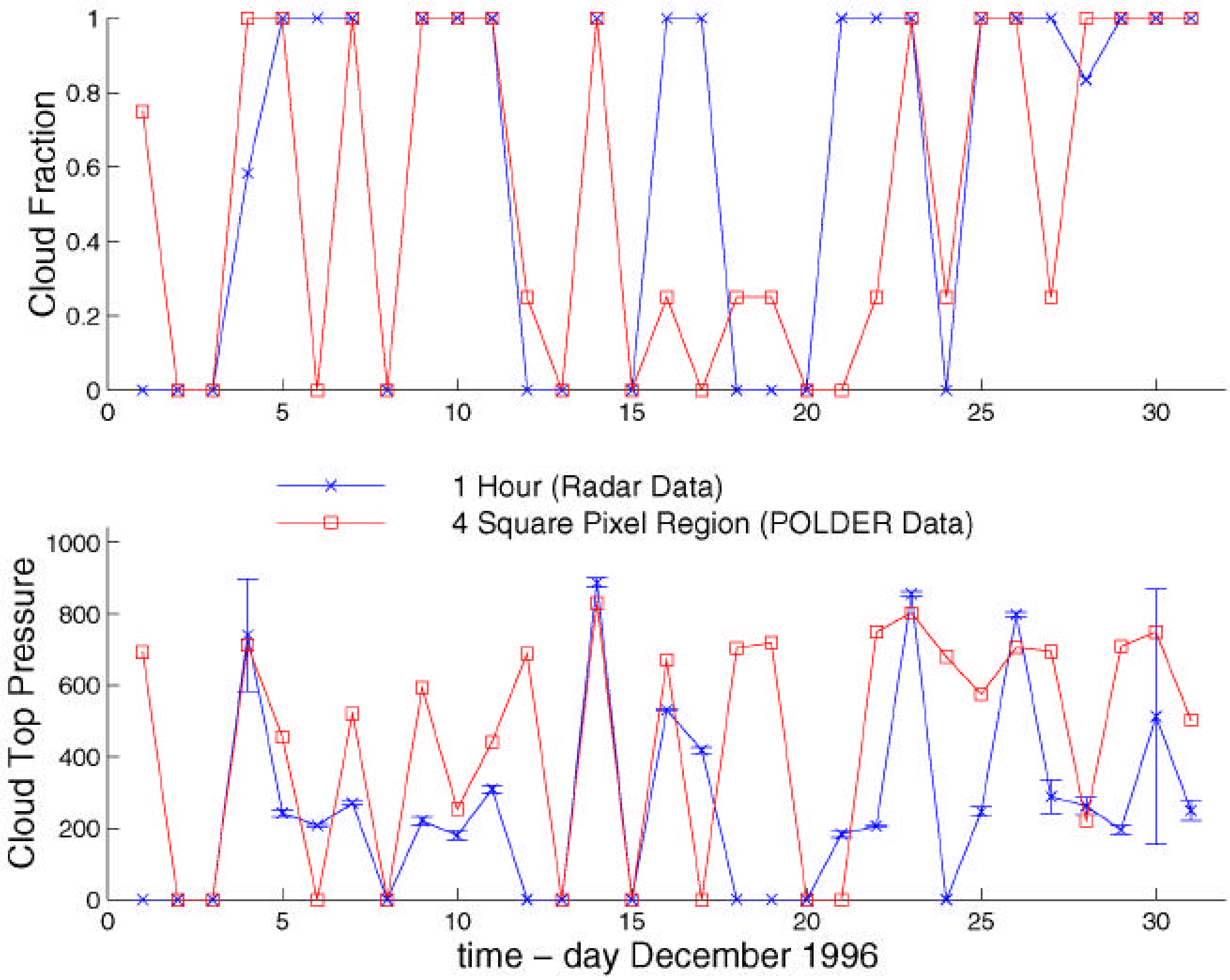

Figure 7.

Cloud Overlap Statistics

The radar time-height data when combined with rawinsonde data can be used to map the radar and lidar detections onto pressure grids more typical of general **(GLOBAL???)** circulation models (GCMs) or numerical weather predictions (NWPs). Figure 8 shows, for example, a 12-hour period of radar data with a GCM-like cloud grid (white boxes) superimposed on top. In this example, the GCM-like cloud map was set "on" only when it was either half filled by radar detections (above the lidar-retrieved cloud base) or if it had more radar detections than the cell above or below it (regardless of the number of detections).

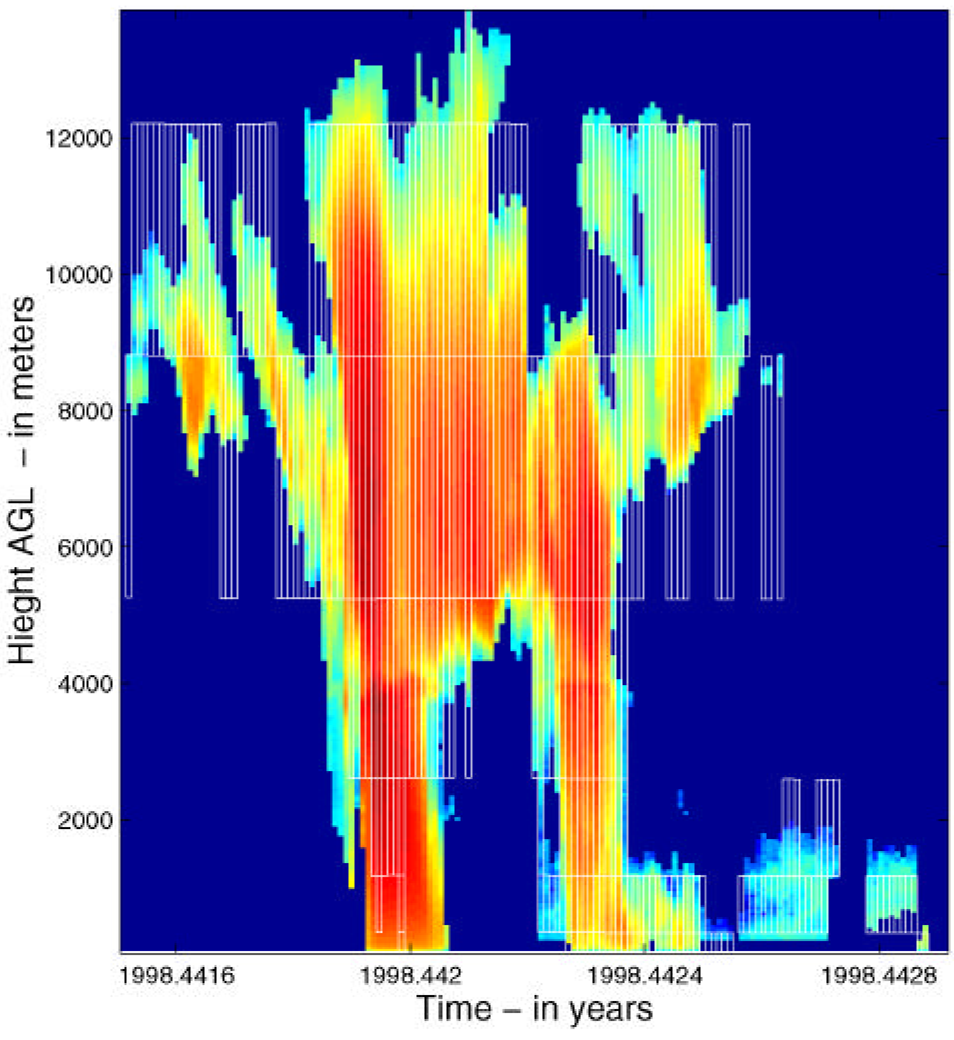

Figure 8.

Using the GCM-like cloud map, one can calculate cloud statistics such as the overlap fraction between various pressure levels. That is, given a cloud fraction for two layers, what fraction of the time is there a cloud in both. Figure 9, for example, depicts the measured result (red circles) and the result that would be obtained using the mixed model (blue crosses).

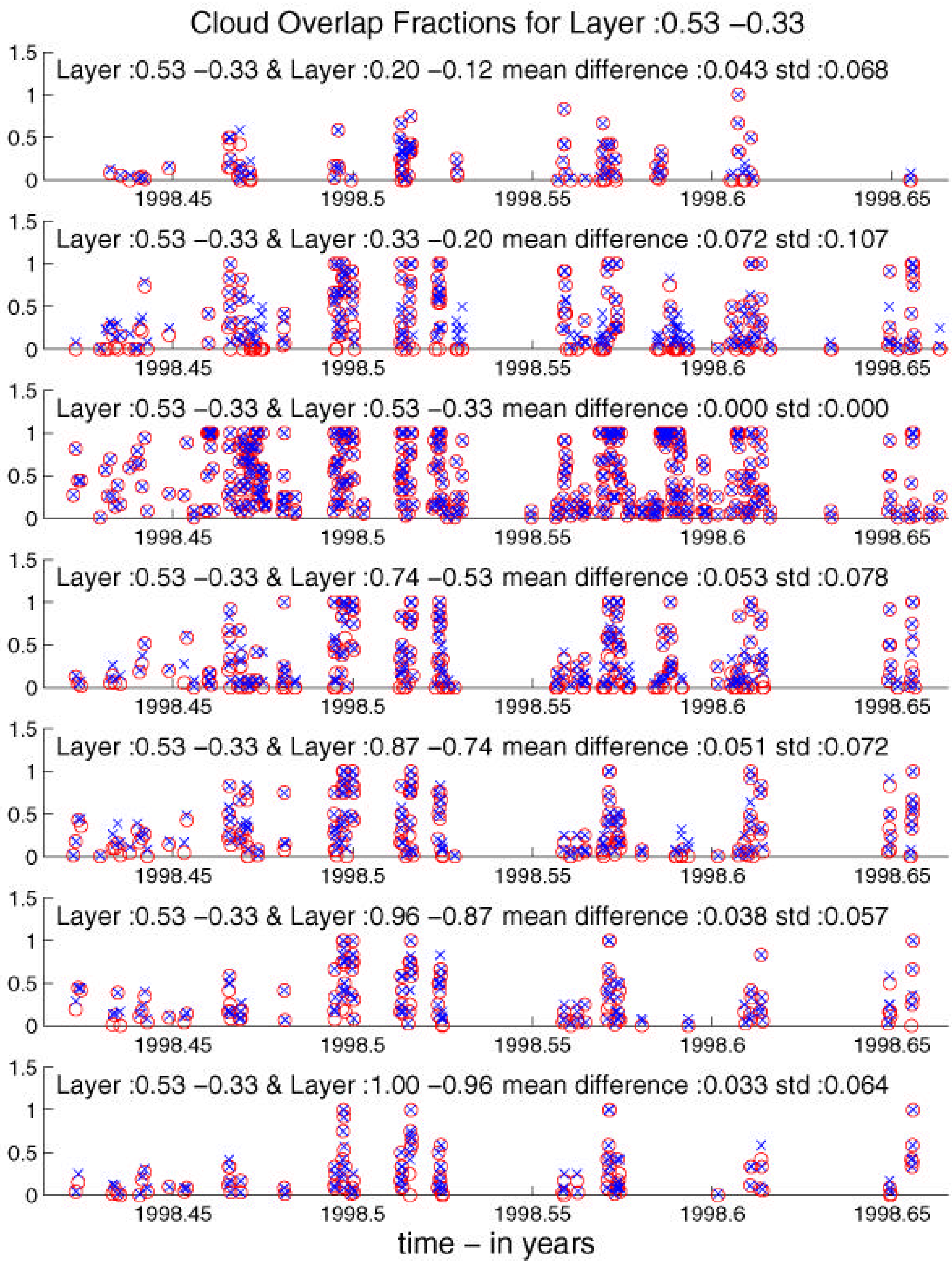

Cloud Overlap Fractions for Layer :0.53 –0.33
Layer :0.53 –0.33 & Layer :0.20 –0.12 mean difference :0.043 std :0.068
Layer :0.53 –0.33 & Layer :0.33 –0.20 mean difference :0.072 std :0.107
Layer :0.53 –0.33 & Layer :0.53 –0.33 mean difference :0.000 std :0.000
Layer :0.53 –0.33 & Layer :0.74 –0.53 mean difference :0.053 std :0.078
Layer :0.53 –0.33 & Layer :0.87 –0.74 mean difference :0.051 std :0.072
Layer :0.53 –0.33 & Layer :0.96 –0.87 mean difference :0.038 std :0.057
Layer :0.53 –0.33 & Layer :1.00 –0.96 mean difference :0.033 std :0.064
1.5
1
0.5
0
1998.45
1998.5
1998.55
1998.6
1998.65
time – in years

Figure 9.

In the mixed model, adjacent layers and layers where all the intervening layers have clouds are assumed to have maximum overlap. If there is an intervening layer without clouds, then random overlap is assumed.

For summer 1998, the mixed-model agrees on average to better than 10% (of the total time) with the radar-inferred cloud overlap. These results are dependant on the pressure level boundaries, the definition used in deciding whether a given pressure cell is cloud filled, and to a lesser degree on the length of time used in calculating the overlap fractions (6 hours in this example).

Summary

The selection of results displayed here show that although there are common features in the 25 months of data analyzed, thus far every month displays some unique characteristics. No statistics tied to derived values of the surface solar cloud forcing or microwave radiometer liquid (or vapor) path were displayed in this paper, but are included in the current database. Instead, we chose to emphasize examples of how this data can be used in analysis of satellite retrievals (e.g., POLDER cloud top pressure) and GCM model parameters (e.g., cloud overlap fractions).